Liquid Crystals
Publication details, including instructions for authors and subscription information:
http://www.informaworld.com/smpp/title~content=t713926090

Twist grain boundary and antiferroelectric smectic C* phases in a new chiral compound

L. Navailles[a]; H. T. Nguyen[a]; P. Barois[a]; N. Isaert[b]; P. Delord[c]
[a] Centre de recherche Paul Pascal, Pessac Cedex, France [b] Laboratoire de Dynamique et Structure des Matériaux Moléculaires, Université de Lille I, Villeneuve d'Ascq Cedex, France [c] Groupe de Dynamyque des Phases Condensées, Université de Montpellier II, Montpellier Cedex 05, France

To cite this Article Navailles, L. , Nguyen, H. T. , Barois, P. , Isaert, N. and Delord, P.(1996) 'Twist grain boundary and antiferroelectric smectic C* phases in a new chiral compound', Liquid Crystals, 20: 5, 653 — 664
To link to this Article: DOI: 10.1080/02678299608031156
URL: http://dx.doi.org/10.1080/02678299608031156

LIQUID CRYSTALS, 1996, VOL. 20, NO. 5, 653-664

Twist grain boundary and antiferroelectric smectic C* phases in a new chiral compound

by L. NAVAILLES, H. T. NGUYEN*, P. BAROIS
Centre de recherche Paul Pascal, Avenue A. Schweitzer, F-33600 Pessac Cedex, France

N. ISAERT
Laboratoire de Dynamique et Structure des Matériaux Moléculaires, Université de Lille I, U.F.R. de Physique, F-59655 Villeneuve d' Ascq Cedex, France

and P. DELORD
Groupe de Dynamyque des Phases Condensées, Université de Montpellier II, U.R.A. 233, F-34095 Montpellier Cedex 05, France.

(*Received 6 October 1994; in final form 10 November 1995; accepted 27 November 1995*)

During the last five years, two new liquid crystalline structures have been obtained with chiral molecules: antiferroelectric smectic C* and Twist Grain Boundary (TGB) smectic phases have received much attention as materials for fundemental studies and for display device applications. Up to now, these two phases have rarely been observed in the same pure compound. In this paper we report the synthesis and studies of a new chiral tolane having the formula:

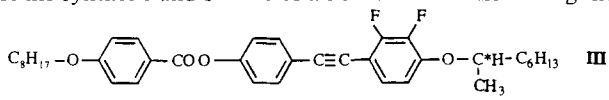

III

It presents for the first time the new TGB_C and antiferroelectric mesophases. Optical microscopic observation and DSC show the sequence:

$$Cr\ S^*_{C_A}\ S^*_{C_{F1}}\ S^*_C\ TGB_C\ TGB_?\ N^*\ BP\,I$$

The low temperature TGB_C phase was identified by miscibility studies with the well known compound $12F_2BTFO_1M_7$ [10] and by X-ray diffraction. The pitch values of the different chiral phases are short and the direction of torsion of the helices of the S^*_C and S^*_{CA} phases are inverse. The electro-optical properties of these tilted phases have also been assessed in the classical SSFLC geometry.

1. Introduction

De Gennes' analogy [1] between smectic A liquid crystals and superconductors was beautifully illustrated in 1988-9 by the discovery of the Twist Grain Boundary (or TGB) smectic phase. Predicted first by Renn and Lubensky [2], the TGB phase appears as the liquid crystal analogue of the Abrikosov flux lattice appearing in type II superconductors: twist penetrates the smectic structure via a twisted lattice of screw dislocations just as magnetic induction penetrates the type II superconductor via a triangular lattice of vortices. As a result, a TGB phase is characterized by the simultaneous observation of smectic layers and of a helical structure of the director as in a cholesteric.

Furthermore, three kinds of TGB phases were predicted in the vicinity of a chiral NAC point, where the cholesteric, smectic A and smectic C* phases meet, namely the TGB^*_A, TGB_C and TGB^*_C phases in which the local ordering is smectic A, tilted smectic C and helical smectic C*, respectively [3].

*Author for correspondence.

The Twist Grain Boundary smectic A phase, TGB_A, was discovered by Goodby *et al.* [4] in 1989 in a series of compounds having the general formula:

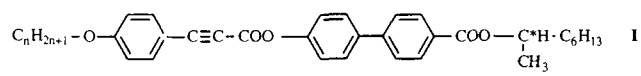

I

For long chain homologues, the observed phase sequence is S^*_C–TGB_A–I. It differs from the sequence predicted by Renn and Lubensky [2], i.e. S_A–TGB_A–N*.

In 1991, Nguyen *et al.* [5] explored the influence of the tolane core (instead of the biphenyl core) and of the substitution in the ring of a 4-alkoxybenzoyloxy group on the stabilization of the TGB_A phase. This phase only shows up with very long alkoxy chains in the reduced phase sequence: S^*_C–TGB_A–I.

0267-8292/96 $12·00

The complete superconductor theoretical sequence (i.e. S_A-TGB_A-N*) was first found by Lavrentovich *et al.* [6] in a mixture of cholesteryl *n*-nonanoate and 4-*n*-nonyloxybenzoic acid in a 7 : 3 weight proportion. Then, it was observed in a pure compound by Slaney *et al.* [7]: in this case the chiral primary alcohol was derived from an L-amino acid. Recently, the S_A–TGB_A–N* phase sequence was observed in three new series in which the chiral chain was derived from (L) lactic acid [8].

In 1992, Bouchta *et al.* [9] synthesized the new series *n*FBTFO$_1$M$_7$ of general formula:

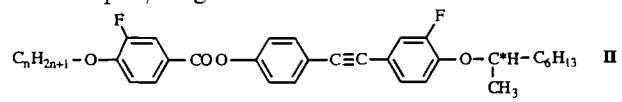

II

Replacing the –COO– linking group between the chiral chain and the core by –O– destabilizes the S_A and TGB_A phases. In order to increase the transverse polarity of the –O– linking group, an electronegative subtituent (fluorine) was introduced in the *ortho*-position to the chiral chain. The transverse polarity is then comparable to that of –COO– and the TGB_A phase is observed in all the members.

Nguyen *et al.* [10] then proposed a new series with two fluorines substituted on the first phenyl ring. The superconductor phase sequence was found for several compounds and the Twist Grain Boundary smectic C phase was discovered and characterized [11].

On the other hand, the study if the antiferroelectric smectic C* phase [12 (a)] (i.e. identical to the smectic O* phase [12 (b-d)] represents another very interesting field of research on chiral liquid crystals. The antiferroelectric smectic C* phase ($S^*_{C_A}$) and other related structures (like the ferrielectric S^*_C or $S^*_{C_{FI}}$ phase) show important properties for potential applications. The synthesis and characterization of new materials exhibiting these two phases is in progress.

In this paper, we present the mesomorphic properties and structural studies of a new material exhibiting both TGB and antiferroelectric smectic C* phases. The formula is:

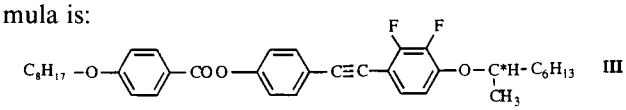

III

or 8BTF$_2$O$_1$M$_7$ for short.

The chemical synthesis is presented in §2. In §3, we examine the mesomorphic properties and those of a binary mixture by optical microscopy and differential scanning calorimetry. The structural studies are reported in §4, together with helical pitch measurements, electro-optical properties and X-ray scattering data.

2. Synthesis

The compound studied is prepared as shown in schemes 1 to 4:

Scheme 1:

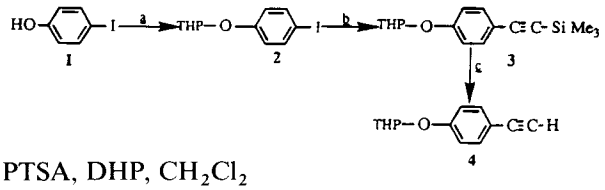

a: PTSA, DHP, CH_2Cl_2
b: Ph_3P, HC ≡ C-$SiMe_3$, $PdCl_2$, $Cu(AcO)_2$; H_2O, Pr_2NH
c: KOH, H_2O, MeOH, THF

Scheme 2:

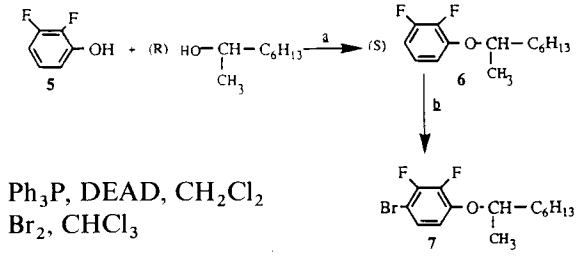

a: Ph_3P, DEAD, CH_2Cl_2
b: Br_2, $CHCl_3$

Scheme 3:

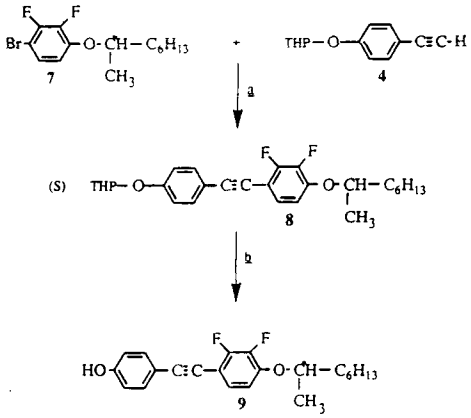

a: Ph_3P, $PdCl_2$, $Cu(AcO)_2$; H_2O, Pr_2NH
b: CH_3OH, PTSA

The 4-octyloxybenzoic acid is prepared following the reaction:

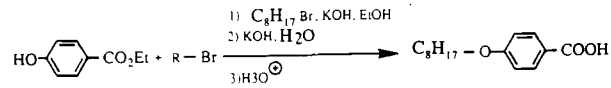

Scheme 4:

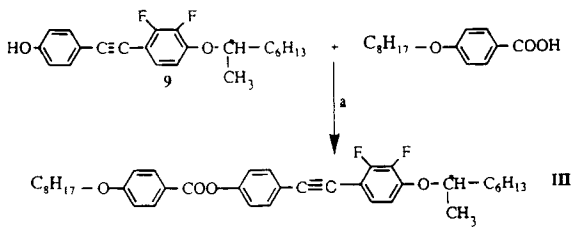

a: DCC, DMAP, CH_2Cl_2
Details of the synthesis are reported in the experimental section.

3. Mesomorphic properties

3.1. *Optical microscopy observations and calorimetric studies*

The transtition temperatures and enthalpies of the new material were determined by thermal optical microscopy (Mettler FP52) and differential scanning calorimetry (DSC Perkin Elmer 7). It exhibits a cholesteric phase (N*), two blue phases (BPI and BPII), twist grain boundary phases (TGB), a classical ferroelectric smectic C* phase (S^*_C) and monotropic ferri-($S^*_{C_{FI}}$) and antiferroelectric ($S^*_{C_A}$) smectic C* phases.

Blue phases are difficult to observe under the polarizing microscope, but easily detected by DSC. Blue phase II (BPII) was obtained with a characteristic iridescent defect texture. We give below the sum of the N* to BP and BP to I transition enthalpies.

The cholesteric phase appears with a focal-conic or Grandjean texture. Between the cholesteric and the classical smectic C* phases we observe another phase with a Grandjean or pseudo-homeotropic texture. Anticipating the structural studies, we identified this helical smectic phase as a twist grain boundary smectic C phase. The temperature range of this phase is about 2°C. The thermogram obtained on heating at a rate of 0·5°C min^{-1} is shown for this compound in figure 1 (*a*). The phase transitions N* to TGB_C and TGB_C to S^*_C are clearly distinguished. The corresponding enthalpy [ΔH (N*–TGB–S^*_C)] is weak. The DSC trace clearly shows a tiny maximum about 0·4°C below the sharp TGB_C–N* transition, see figure 1 (*a*), which suggests the existence of a phase transition within the TGB_C domain. This anomaly will be discussed later in § 3.2. For the moment, we choose for convenience to denote as TGB_1 the low temperature TGB_C and as TGB_2 the high temperature TGB_C.

The classical ferroelectric smectic C* phase appears with a striated fan-shaped or pseudo-homeotropic texture. Upon cooling, the ferri- and antiferro-electric smectic C* phases appear at around room temperature, figure 1 (*b*). Note that the twist grain boundary smectic C and the antiferroelectric smectic C* phases appear for the first time in the same phase sequence with the cholesteric phase.

The phase sequence is given below: (heating rate 0·5°C min^{-1})

Cr 52·4 ($S^*_{C_A}$ 39·7 $S^*_{C_{FI}}$ 40·7) S^*_C 86·2 TGB_1 87·5 TGB_2 87·9 N* 124·4 BP 124·8 I (ΔH kJ mol^{-1})

* 25·2 (0·270) * 0·045 * 0·485 * 0·566 *

3.2. *Mixture studies*

Observation of racemic $8BTF_2O_1M_7$ under the optical polarizing microscope reveals the following phase sequence: S_C 90·4 N 127·7 I. The TGB phase disappears

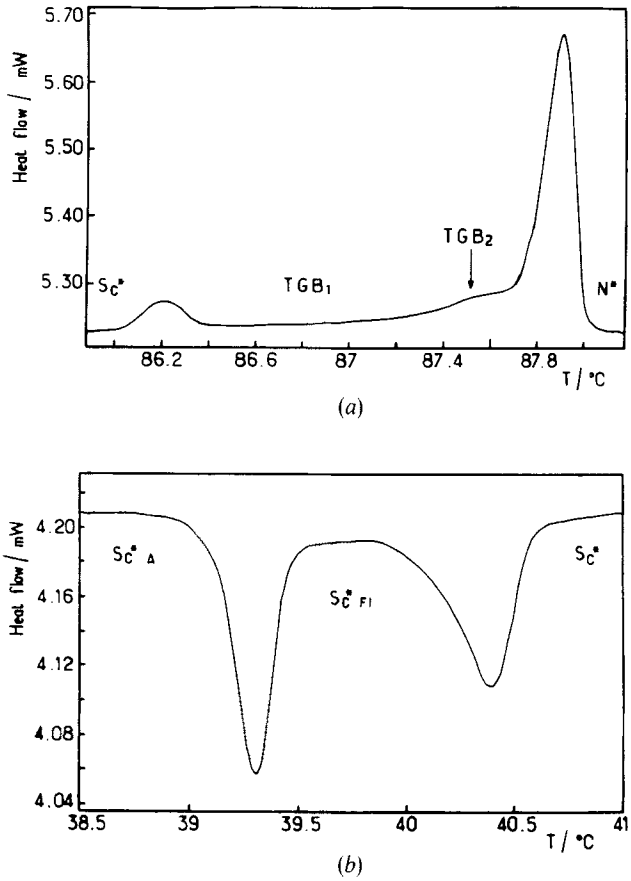

Figure 1. (*a*) Differential scanning calorimetry thermogram of $8BTF_2O_1M_7$ (S). Heating rate 0·5°C min^{-1}. Phase sequence: S^*_C–TGB_1–TGB_2–N*. (*b*) Differential scanning calorimetry thermogram of $8BTF_2O_1M_7$ (S). Cooling rate 0·5°C min^{-1}. Phase sequence: S^*_C–$S^*_{C_{FI}}$–$S^*_{C_A}$.

to the benefit of a smectic C phase, which is consistent with a tilted TGB phase. Let us point out that in the racemic material, the $S^*_{C_{FI}}$ and $S^*_{C_A}$ also disappear. The former exists only with a high optical purity and the existence of the latter depends on the odd–even length both of the chiral chain and the alkoxy chain.

We have also studied the phase miscibility between $8BTF_2O_1M_7$ (S) and the well characterized compound $12F_2BTFO_1M_7$ (S) of formula:

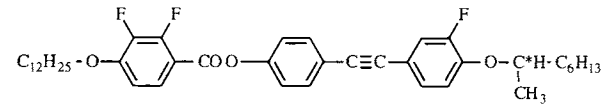

and phase sequence [10].

Cr 36·6 S^*_C 102·8 TGB_C 103 N* 110·5 BP 111·7 I

The temperatures of transition and the corresponding enthalpies were obtained by DSC studies. Storage and addition of several scans were used in order to optimize the signal to noise ratio. The TGB_1–TGB_2 transition

remains in the DSC scans for weight fractions of $12F_2BTFO_1M_7$ (S) as high as 70% (see the table and figure 2). The data also show that the low temperature TGB_1 phase of $8BTF_2O_1M_7$ (S) is miscible with the TGB_C phase of pure $12F_2BTFO_1M_7$ (S).

4. Structural studies

4.1. *Helical pitch measurements*

Twist measurements on the cholesteric and TGB phases were performed using a Grandjean-Cano wedge [13(a-c)]. Excellent planar orientation (figure 3) is obtained in a wedge made of very clean rubbed glass plates forming a small angle ($\alpha \cong 0{\cdot}25°$). The material is introduced by capillarity in the isotropic phase and cooled down quickly to the cholesteric phase. The observation of the classical Grandjean-Cano texture shows that the helix direction is perpendicular to the glass plates (figure 6).

Figure 4 represents the evolution of the pitch with temperature in the N*, TGB_C and classical smectic C* phases for $8BTF_2O_1M_7$ (S). The pitch is very short in the cholesteric phase: it increases continuously from 0·22 μm just below the isotropic phase to 0·28 μm just above the N*–TGB_C transition. The lattice of Grandjean–Cano lines expands regularly in the N* phase, but breaks up at the N*–TGB_C transition to rearrange in the TGB_C phase with a larger spacing and different reflected colours. This is typical of a discontinuous jump in the helical pitch at the N*–TGB_C transition. The discontinuity is estimated to be from 0·28μm at 90°C in the N* phase to 0·4 μm at 89·4°C in the TGB_C phase.

In the S_C^*, $S_{C_A}^*$ and $S_{C_{FI}}^*$, on the other hand, the helical axis is perpendicular to the smectic layers and the formation of Grandjean-Cano textures requires homeotropic boundary conditions. Figure 5 shows the pitch (P) versus temperature situation in these phases. The measurements were again performed using calibrated wedges ($\alpha = 0{\cdot}25°$) in which homeotropic alignment was generally easily acheived with clean gently rubbed glass plates.

In the S_C^* phase, we observed Grandjean-Cano steps sharply coloured by selective reflection of light. In transmitted light, samples were perfectly black and the steps were invisible. The pitch values are very weak: from 0·4 μm at 85°C just below the TGB_C–S_C^* transition (giving selective reflection of red light) to 0·27 μm at 75°C. Meanwhile, the reflected wavelength λ (related to the pitch P by $\lambda = nP$, where n is the average refractive index) traverses the whole visible spectrum from red to violet. At lower temperatures, the pitch keeps decreasing down to remarkably low values: from 0·27 μm at 75°C to less than 0·12 μm at 43°C. A second, but less luminous reflected visible spectrum is then observed from red to violet. It corresponds to a second order reflection $\lambda = 2nP$. At the S_C^*–$S_{C_{FI}}^*$ transition (42·2°C), two successive visible spectra are crossed (from violet to red) denoting a very sharp increase of the pitch. This behaviour is qualitatively represented by the open circles in figure 5.

In the $S_{C_A}^*$ phase, at the $S_{C_{FI}}^*$–$S_{C_A}^*$ transition (41·2°C), a single visible spectrum ($\lambda = np$) is quickly crossed indicating that the pitch decreases from large values to values lower than 0·27 μm. In the $S_{C_A}^*$ phase, we could not measure the pitch with accuracy because neither reflected

Transition temperatures (°C) and corresponding enthalpies ($J g^{-1}$) of the mixtures of $8BTF_2O_1M_7$ (S) [8BTF2] and $12F_2BTFO_1M_7$ (S) [12F2].

$12F_2$	$8BTF_2$	S_C^*	TGB_1	TGB_2	N*
0%	100%	● 86·2	● 87·5	● 87·9	●
		● (0·074)[a]	● (0·799)[b]		●
10%	90%	● 86·1	● 87·9	● 88·1	●
		● (0·057)[a]	● (0·616)[b]		●
20%	80%	● 86·9	● 89	● 89·34	●
		● (0·032)[a]	● (0·522)[b]		●
50%	50%	● 92	● 93·95	● 94·26	●
		● (0·026)[a]	● (0·446)[b]		●
60%	40%	● 93·8	● 95·38	● 95·56	●
		● (0·028)[a]	● (0·371)[b]		●
70%	30%	● 96·3	● 97·5	● 97·63	●
		● (0·031)[a]	● (0·324)[c]	—	●
80%	20%	● 98·41	● 99·31	—	●
		● (0·061)[a]	● (0·259)[c]	—	●
90%	10%	● 100·33	● 100·93	—	●
		● (0·063)[a]	● (0·222)[c]	—	●
100%	0%	● 103·4	● 103·77	—	●
		● (0·058)[a]	● (0·197)[c]	—	●

[a] ΔH (S_C^*–TGB_1), [b] ΔH (TGB_1–TGB_2–N*), [c] Δh (TGB_1–N*).

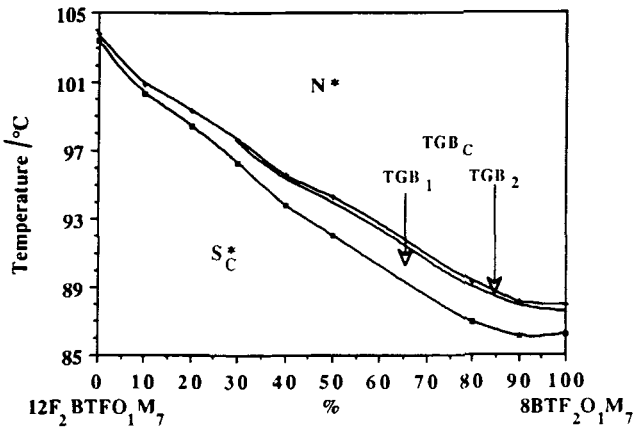

Figure 2. Miscibility phase diagram of binary mixtures (wt %) of $12F_2BTFO_1M_7$ (S) and $8BTF_2O_1M_7$ (S). The TGB_1–TGB_2 transition within the TGB_C domain is detected by DSC only.

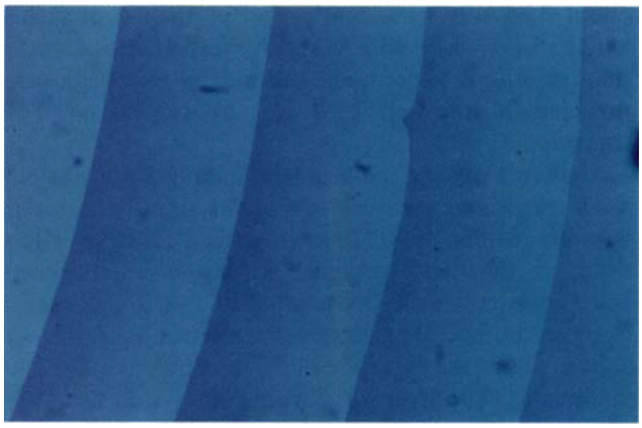

Figure 3. Photographs of the Cano wedge with planar boundary conditions. Grandjean–Cano lines in the N* phase of $8BTF_2O_1M_7$.

colours nor good Grandjean–Cano steps could be observed.

No measurements were made for the ferrielectric phase. The evolution of the pitch can however be inferred from the observation of pseudo-homeotropic droplets exhibiting periodic fringes of equal thickness. The twist ($1/P$) seems to vary continuously and change sign in the $S^*_{C_{FI}}$ domain. The handedness of the twist was deducted from the analysis of the rotatory power or the reflection of circularly polarized light. The helix is right handed in the S^*_C phase and left handed in the $S^*_{C_A}$ phase.

4.2. *Electro-optical properties*

We have studied the electro-optical properties of $8BTF_2O_1M_7$ (S) in the Surface Stabilized Ferroelectric

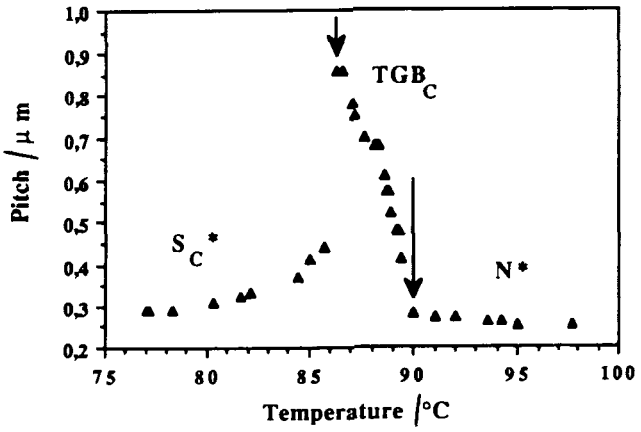

Figure 4. Helical pitch for the N*, TGB and classical S^*_C phases versus temperature.

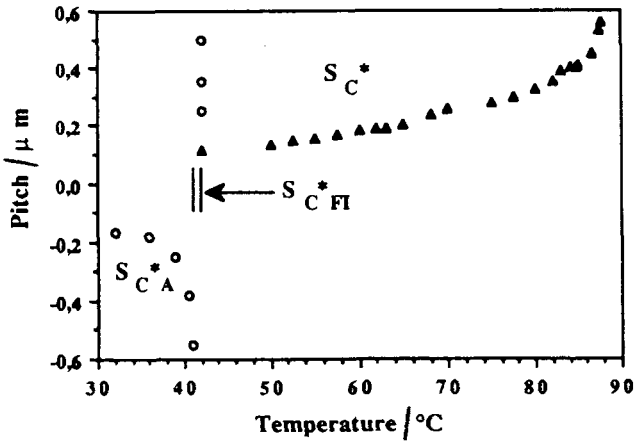

Figure 5. Helical pitch for the S^*_C, $S^*_{C_{FI}}$ and $S^*_{C_A}$ phases versus temperature.

Figure 6. Photograph of the Cano wedge with planar boundary conditions in a weak temperature gradient. Grandjean–Cano lines are visible in both phases at the N*–TGB_C transition of $8BTF_2O_1M_7$ (blue colour for the N* phase and yellow for the TGB_C phase).

Liquid Crystal configuration [14, 15]. The sample thickness of 5 μm was thin enough for SSFLC measurements, because the helical axes of the S_C^* and $S_{C_A}^*$ phases were parallel to the surfaces. For example with a cell thickness of 50 μm one can measure the polarization, but with a high field.

Figures 7 (*a*) and 7 (*b*) show the evolution of the spontaneous polarization and response time with rms voltage and as a function of frequency 80°C (S_C^* phase). The response time can be defined as:

$$\tau = \int i_p(t)\,dt/2i_p(\tau_m),$$

where $i_p(t)$ is the polarization current and τ_m is the time between the field reversal and the maximum of the current peak. This response time was independent of the preparation. Both are independent of frequency (100 to 2000 Hz). The voltage corresponding to saturation was about 30 V. At low temperatures, in the antiferroelectric smectic C* phase we observed, figures 8 (*a*) and 8 (*b*), a threshold field of 30 V (/5 μm) characteristic of this phase.

In the TGB_C phase, at low field, (say below 10 V/5 μm), with planar boundary conditions, the measured polarization is zero. In this geometry, the field is applied along the pitch direction *P*.

Above some threshold field of the order 10 V/5 μm, a polarization current is detected, but a new optical texture develops. At high field (> 20 V/5 μm) the texture is very similar to a classical, well aligned S_C^* texture. We interpret this observation as a field induced TGB_C–unwound S_C^* transition. However, just above the threshold field, the sample exhibits striated domains typical of a twisted structure with the helical axis parallel to the cell walls (i.e. perpendicular to the applied field). We believe that the helical direction tips over from parallel to perpendicular to the applied field at the threshold, whereas the remaining TGB helix unwinds at higher field. No evidence of longitudinal (i.e. along *P*) ferroelectricity of the TGB_C phase is thus found, unlike that expected from the RL model. The reported observations are rather consistent with a helielectric TGB_C structure (i.e. with a polarization component perpendicular to the pitch direction and precessing about it) as suggested by recent structural experiments [16].

Figures 9, 10 and 11 show the evolution of the saturated polarization, response time and tilt angle with temperature. Between 80 and 55°C, we worked with 40 V and 20 Hz. At low temperatures (< 55°C) we used 55 V and 20 Hz. For the tilt angle measurements, the frequency was 0·2 Hz and the saturation field was changed to 35 V at high temperature to 60 V in the $S_{C_A}^*$ phase. We observed a high polarization (90 nC cm^{-2}), a slow response time and a saturated tilt angle of 31°C. Below 65°C, it is interesting to note that the tilt angle decreases slightly. The polarization also decreases from 88 nC cm^{-2} to 70 nC cm^{-2}.

4.3. *X-ray diffraction*

X-ray scattering experiments were performed on the $8BTF_2O_1M_7$ (S) homologue. Powder samples were prepared in 1 or 1·5 mm diameter Lindemann capillaries. The scattered intensity was collected with a 2θ goniometer. The temperature was controlled within a 10 mK accuracy. The experiments were performed using the CuK_α radiation of an 18 kW rotating anode X-ray generator [10]. A flat pyrolytic graphite (0 0 2) monochromator delivered a $0{\cdot}5 \times 2\,mm^2$ beam onto the sample. The scattered radiation was analysed by 0·65 mm slits. The horizontal resolution was then 8×10^{-3} Å^{-1} FWHM. Figure 12 shows the evolution of the layer spacing ($d = 2\pi/q_o$) with temperature upon cooling.

In the cholesteric phase, broad reflections (i.e. larger than the resolution function, see inset of figure 12) indicate a short range smectic order. The layer spacing of about 35·4 Å is significantly shorter than a molecular length (for $n = 8,1 = 43{\cdot}1$ Å) and suggests smectic C rather than smectic A short range order. The smectic correlation length is about 65 Å just above the N*–TGB transition.

The layer spacing jumps down about 0·5 Å at the N*–TGB transition, then decreases continuously with temperature within the TGB region. The local smectic C order is thus well established in the TGB phases. Furthermore, a little broadening of the Bragg peak is observed in the TGB_C phases (see inset of figure 12). We ascribe this to the finite size of the smectic slabs along the pitch axis. This effect was earlier observed in the TGB_C phases of the $nF_2BTFO_1M_7$ series [10]. A few data points were recorded in the TGB_2 region to distinguish a possible TGB_2–TGB_1 transition.

A small discontinuity in the layer spacing was detected at the TGB_C–S_C^* transition. The layer spacing reaches a minimum in the ferroelectric S_C^* phase and starts to increase below 70°C. The slope of the variation changes at the S_C^* to $S_{C_{F_I}}^*$ and $S_{C_{F_I}}^*$ to $S_{C_A}^*$ transitions. The layer spacing always remains much shorter than the molecular length. The Bragg peaks are resolution limited in all the S_C^* phases (ferro-, ferri- and antiferro-electric).

4.4. *Reciprocal space structure*

X-ray experiments performed on the TGB_C phases of the $nF_2BTFO_1M_7$ series [10, 11] have shown that the smectic layers are tilted relative to the pitch axis [16]. Such a structure differs from the model of Renn and Lubensky for the TGB_C phase [3, 17]. Assuming that the director remains perpendicular to the pitch axis as in the

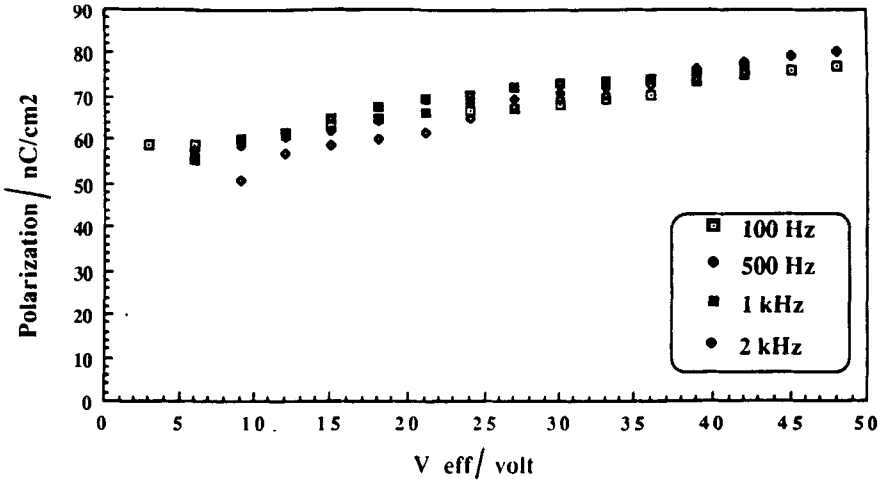

(*a*)

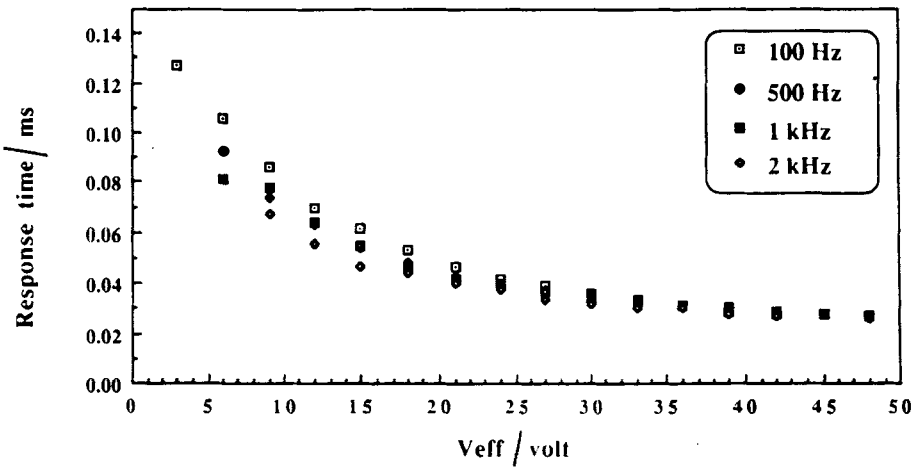

(*b*)

Figure 7. (*a*) Spontaneous polarization versus effective field and frequency at 80°C (S^*_C phase of $8BTF_2O_1M_7$ (S)). (*b*) Response time versus effective field and frequency at 80°C (S^*_C phase of $8BTF_2O_1M_7$ (s)).

cholesteric phase, this result implies that the electric polarization borne by each smectic block is also perpendicular to the pitch axis and precesses about it.

The X-ray diffraction experiments were performed likewise on well aligned samples of the $8BTF_2O_1M_7$ compound to check whether the TGB_C phase is of the Renn type or similar to the TGB_C phase of the $nF_2BTFO_1M_7$ series.

Well aligned samples were prepared as described in [11] between thin (~50 mm) flat pieces of polymer-coated and undirectionally buffed glass. The thickness of the cells was fixed by calibrated spacers (25 μm gold wires). The cells were filled by capillarity in the isotropic phase. The alignment was achieved in the cholesteric phase and controlled under a microscope: planar boundary conditions led to characteristic Grandjean–Cano textures. The cells were then introduced in a two stage oven (±10 mK accuracy) mounted on the 4-circle X-ray spectrometer. X-ray scattering experiments were performed using the CuK_α radiation of an 18 kW rotating anode X-ray generator (Rigaku RO-200). A flat pyrolytic graphite (002) monochromator delivered a $1 \times 1\,mm^2$ beam on to the sample. The scattered intensity was analysed by a $1 \times 2\,mm^2$ vertical slit and collected by a scintillator. The scattering vector **Q** is defined by the axes Q_x, Q_y and Q_z (inset of figure 13). ω and χ are the rocking angles about the vertical (Q_y) and horizontal (Q_x) axes, respectively. The in-plane resolution of the spectrometer was

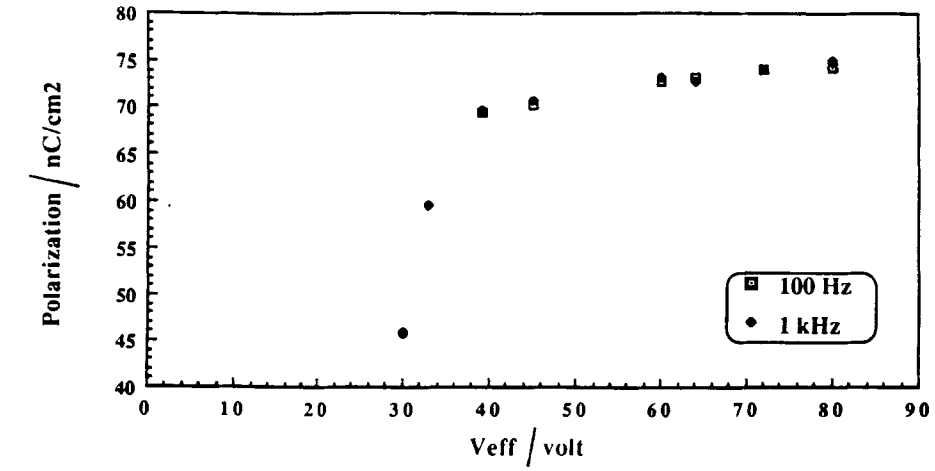

(*a*)

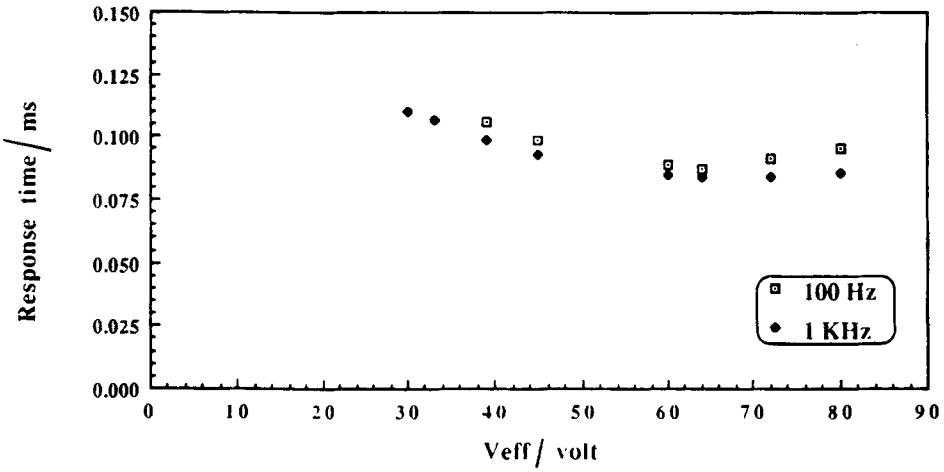

(*b*)

Figure 8. (*a*) Spontaneous polarization versus effective field and frequency at 37°C ($S^*_{C_A}$ phase of $8BTF_2O_1M_7$ (S)). (*b*) Response time versus effective field and frequency at 37°C ($S^*_{C_A}$ phase of $8BTF_2O_1M_7$ (s)).

$\Delta Q_z = 1{\cdot}0\ 10^{-2}$ Å^{-1} (FWHM) in the longitudinal direction. The angular vertical resolution $\Delta\chi$ defined by the 2 mm vertical slits was 13 degrees (FWHM).

The pitch axis $\hat{x}$ was placed along the horizontal direction Q_x of the spectrometer. Cooling down from the cholesteric phase, rocking curves (omega scans) were recorded for the TGB_C phase at constant momentum transfer Q. Figure 13 shows a typical ω scan at $T = 88{\cdot}70$°C (i.e. about 0·3°C below the N*–TGB_C transition) and $Q = 0{\cdot}181$ Å^{-1}. It exhibits two sharp peaks at positions $\omega_L = \pm 16{\cdot}2$ degrees. This structure is similar to the one observed for the TGB_C phase of the $nF_2BTFO_1M_7$ series: the layers are tilted at an angle $\omega_L = \pm 16{\cdot}2$ degrees relative to the pitch axis. The two peaks can be fitted to Lorentzian profiles of width 5 degrees (FWHM).

The tilt angle of the layers has been recorded as a function of temperature throughout the TGB_C domain (figure 14). No qualitative difference was found between the two TGB_C phases: both have tilted layers. The tilt angle ω_L seems to be fairly constant (about $15{\cdot}9 \pm 0{\cdot}1$ degrees) in the high temperature TGB_C, whereas it increases from 15·9 degrees to 22 degrees on cooling in the low temperature TGB_C.

Azimuthal rotations about the Q_x axis (χ scan) at constant ω_L were performed in the two TGB_C regions to investigate the commensurability, i.e. the ratio $q = 2\pi/\Delta\Theta$. If q is rational, the TGB_C is commensurate; the reciprocal lattice is a pair of rings of equi-spaced Bragg spots which produces oscillating χ scans. If on the other hand, q is irrational, the TGB_C is incommensurate; the reciprocal space is formed by two uniform rings, and χ

scans exhibit a constant intensity. In practice, due to the limited angular resolution in χ (13 degrees FWHM), simple integral values of q only may give oscillating χ scans.

A few χ scans were recorded at different temperatures: at 88·90°C in the high temperature TGB_C phase, the scattered intensity $I(\chi)$ is constant, whereas in the low temperature TGB_C, the signal oxcillates. The period corresponds to 11 blocks per pitch and no evolution was observed from 88·70 to 88·00°C. Note that this number corresponds to a fairly high value of the grain boundary angle $\Delta\Theta = 32{\cdot}7$ degrees. It is tempting to conclude that the high and low temperature TGB_C are incommensurate and commensurate, respectively. We cannot rule out however experimental artifacts such as an angular mosaic (or a larger value of q) smearing out the modulation of the χ scans in the high temperature phase.

In conclusion, X-ray diffraction experiments on well aligned samples have shown that the two TGB_C phases have the same structure as previously reported TGB_C phases: the smectic layers are tilted. Experimental observations are consistent with the existence of a commensurate TGB_C–incommensurate TGB_C transition. Further experimental work is however needed to confirm this point.

5. Conclusion

In this paper, we present the mesomorphic properties of a new compound with the general formula $8BTF_2O_1M_7$ (S). The phase sequence I–BP–N*–TGB_C–S^*_C–$S^*_{C_{FI}}$–$S^*_{C_A}$–Cr is found with classical textures. Cholesteric and antiferroelectric phases are found in the same sequence for the first time. The ferri- and antiferroelectric phases appear on cooling to around room temperature.

The thermograms obtained on heating suggest the existence of a phase transition within the TGB_C domain. However, no discontinuity is observed at this transition either using helical pitch measurements or X-ray scattering.

At this stage, it is interesting to note that the pitch values of the different phases (N*, TGB_C, S^*_C) are very short. This observation seems to be related to the existence of the ferri- and antiferro-electric phases. The rotatory power changes sign in the ferrielectric smectic C* phase. The layer spacing as a function of temperature and the electro-optical properties are also reported. The results are on the whole similar to those for other series.

6. Experimental

The infrared spectra were recorded using a Perkin Elmer 783 spectrophotometer and the NMR spectra with a Bruker 270 MHz spectrometer. The compound gives satisfactory elemental analyses. The optical purity of the starting chiral alcohol was 99% (Aldrich) and the chemical purity of the final compound was more than 99% as given by HPLC.

6.1. *(R)-1-(1-methylheptyloxy)-2,3-difluorobenzene(3)*

To a cooler (ice bath) solution of 2,3-difluorophenol (11·6 g, 89·2 mmol), (S)-2-octanol (11·6 g, 89·2 mmol) and TPP (25 g, 94 mmol) in CH_2Cl_2 (200 ml) was added dropwise diethyl azodicarboxylate (DEAD) (17 g, 97·6 mmol). The solution was then stirred at room temperature for 3 h. The solution was filtered, evaporated and chromatographed on silica gel with a (95:5) heptane:ethyl acetate mixture as eluent. Yield: 15·3 g (71

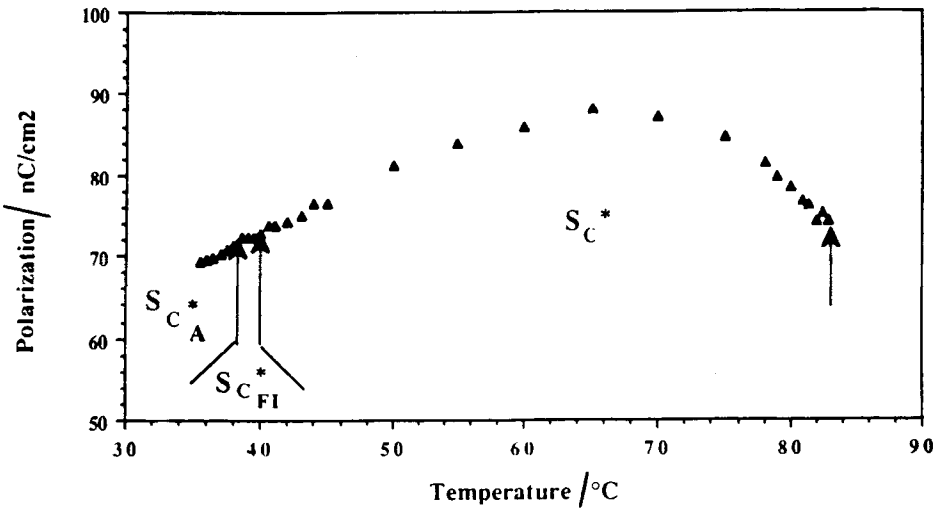

Figure 9. Spontaneous polarization versus temperature for the $8BTF_2O_1M_7$ (S) homologue.

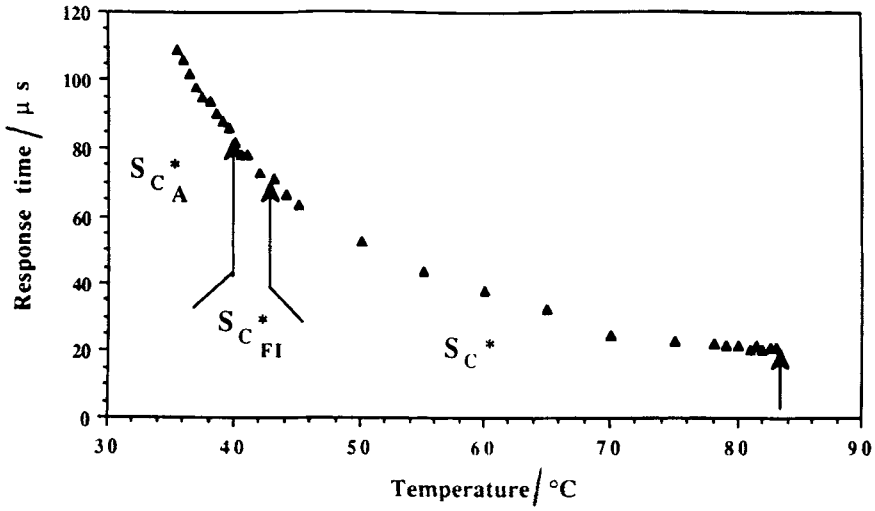

Figure 10. Response time versus temperature for the $8BTF_2O_1M_7$ (S) homologue.

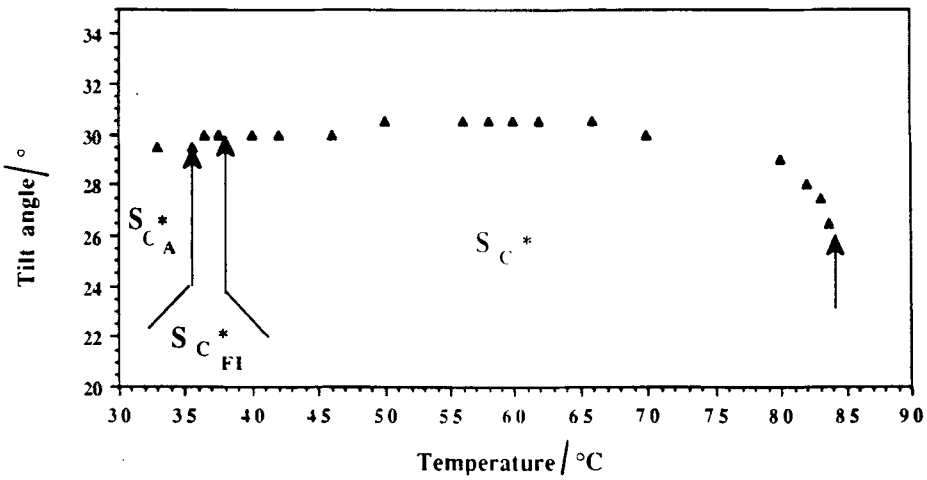

Figure 11. Tilt angle versus temperature for the $8BTF_2O_1M_7$ (S) homologue.

per cent). 1 H NMR ($CDCl_3$, d):0·89 (t, 3H, CH_3 of C_6H_{13}), 1·3 (m, 6H, $3CH_2$), 1·38 (d, 3H of CH_3–CH), 1·6–1·8 (m, 2H, OCH–CH_2), 4·3 (m, 1H, CH–CH_3), 6·8–7·5 (m, 3H arom).
IR (Nujol): 1620, 1220, 960 cm^{-1}.

6.2. *(R)-4-(1-methylheptyloxy)-2,3-difluoro-1-bromobenzene (4)*

To a solution of **3** (30·7 g, 0·127 mol) in anhydrous $CHCl_3$ (400 ml) was added dropwise a solution of Br_2 (20 g, 0·125 mol) in $CHCl_3$ (40 ml) at RT. The resultant solution was stirred overnight and then added to H_2O (500 ml). The organic layer was separated off, washed with diluted Na_2CO_3 solution and H_2O and then dried over anhydrous Na_2SO_4. The solvent was removed by evaporation under reduced pressure. The desired compound was purified by chromatography on silica gel using a (95:5) heptane:ethyl acetate mixture as eluent. Yield: 30 g (73·3 per cent).
IR (Nujol): 2930, 1630, 1280 cm^{-1}.

6.3. *(R)-2,3-difluoro-4-(1-methylheptyloxy)-4'-hydroxytolane (6)*

In a 250 ml round-bottomed flask were placed (4-tetrahydropyranyloxy)phenylacetylene [9] (12 g, 0·06 mol), compound **4** (21·2 g, 0·066 mol), TPP (1·5 g, 5·7 mmol) and dipropylamine (250 ml), under nitrogen. The mixture was stirred and heated in an oil bath at 30°C until complete dissolution. Then the catalyst $PdCl_2$ (170 mg, 0·9 mmol) and $Cu(AcO)_2$:H_2O (190 mg, 0·9 mmol) were added and the solution was gradually heated to 100°C and maintained at this temperature for 4 h. After cooling to room temperature, the salt was removed by filtration and washed well with ethyl acetate. The filtrate was

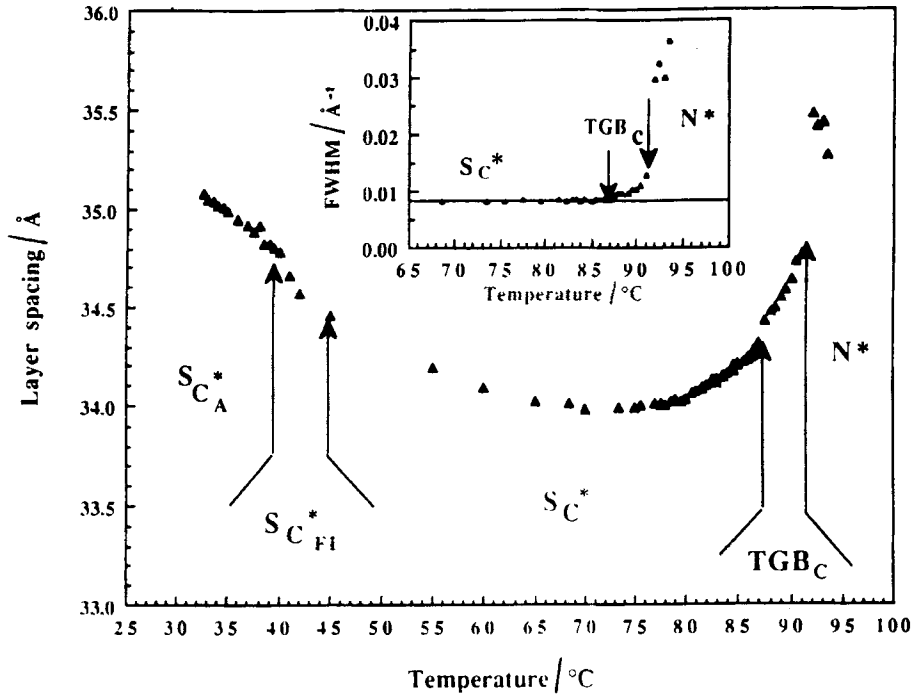

Figure 12. Layer spacing versus temperature for the $8BTF_2O_1M_7$ (S) homologue upon cooling. Inset shows a plot of the peak width versus temperature. Solid line is the instrumental resolution (0·008 $Å^{-1}$). Peaks are resolution limited in the chiral smectic C phase only.

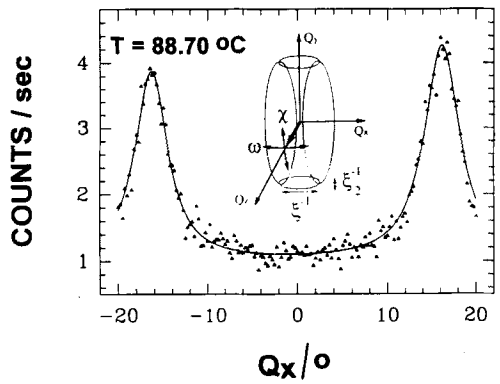

Figure 13. Plots of the X-ray intensity scattered along the direction Q_x of the screw axis through the Bragg maximum at $Q_z = 0{\cdot}181$ $Å^{-1}$. Scan at $T = 88{\cdot}70°C$, about 0·3°C below the N*–TGB_C transition. The solid line is a fit to lorentzian profiles of width 5 degrees (FWHM). Inset shows the scattering geometry: ω and χ scans are rotations about the Q_y and Q_x axes, respectively.

evaporated and the residue hydrolysed with diluted hydrochloric acid (100 ml of 10%), and then shaken with ethyl acetate. The organic phase was dried over anhydrous Na_2SO_4, filtered and evaporated. The intermediate compound **5** (16 g) was obtained and dissolved in CH_2Cl_2 (100 ml) and CH_3OH (180 ml). To this solution was added PTSA (0·4 g) and the mixture stirred at RT for

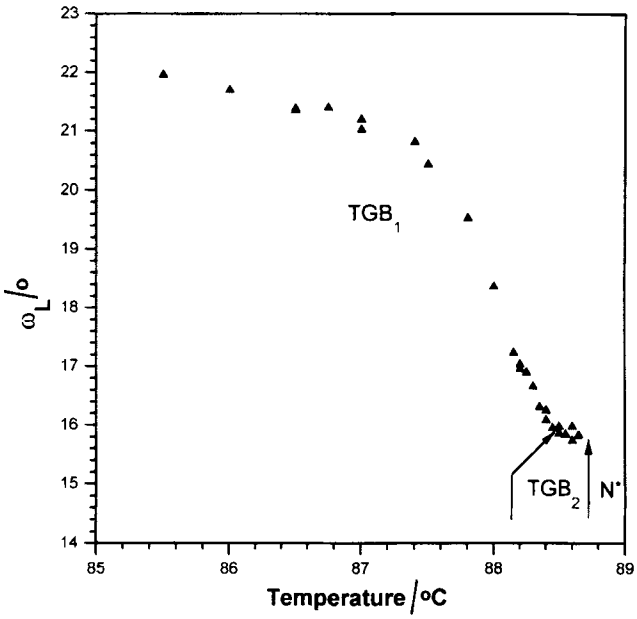

Figure 14. Tilt angle ω_L of the layers relative to the screw axis versus temperature at the N*–TGB_C transition for $8BTF_2O_1M_7$.

1 h. The solvent was removed and the pure phenol was obtained by chromatography on silica gel using (8:2) heptane:ethyl acetate mixture as eluent. Yield 10·3 g (48 per cent).
IR (Nujol): 3240, 1650, 1230, 1130 cm^{-1}.

6.4. *(R)-2,3-difluoror-4-(1-methylheptyloxy)-4'-(octyloxybenzoyloxy)tolane*

To a solution of phenol **6** (0·72 g, 2 mmol) in CH_2Cl_2 (5 ml) was added dicyclohexylcarbodiimide (DCC) (0·45 g, 2·2 mmol), DMAP (40 mg) and 4-octyloxybenzoic acid (0·55 g, 2·2 mmol). The resulting solution was stirred at RT overnight. The solution was filtered, evaporated and the residue chromatographed on silica gel with toluene as eluent. The pure compound was recrystallized from absolute ethanol. Yield: 0·8 g (63 per cent). 1H NMR ($CDCl_3$, d): 0·85 (t, 6H, $2CH_3$), 1·23 (m-16 H, $8CH_2$), 1·32 (d, 3H, CH_3–CH), 1·8 (m, 4H $2CH_2$ β), 4·03 (t, 2H, OCH_2), 4·3 (m, 1H, CH–CH_3), 6·8–8·2 (m, 10H arom.).
IR (Nujol): 1730, 1280, 1210 cm^{-1}

The authors would like to thank Professor C. Destrade and P. Cluzeau for stimulating discussions and their interest in this work.

References

[1] De Gennes, P. G., 1972, *Solid State Commun.*, **10,** 753.
[2] Renn, S. R., and Lubensky, T. C., 1988, *Phys. Rev. A*, **38,** 2132.
[3] Renn, S. R., 1992, *Phys. Rev. A*, **45,** 953.
[4] Goodby, J. W., Waugh, M. A., Chin, E., Pindak, R., and Patel, J. S., 1989, *J. Am. chem. Soc.*, **111,** 8119.
[5] Nguyen, H. T., Twieg, R. J., Nabor, M. F., Isaert, N., and Destrade, C., 1991, *Ferroelectrics*, **121,** 187.
[6] Lavrentovich, O. D., Nastishin, Y. A., Kulishov, V. I., Narkevich, Y. S., Tolocka, A. S., and Shiyanovskii, S. V., 1990, *Europhys. Lett.*, **13,** 313.
[7] Slaney, A. J., and Goodby, J. W., 1991, *J. Mater. Chem.*, **1,** 5.
[8] Navailles, L., Nguyen, H. T., Barois, P., Destrade, C., and Isaert, N., 1993, *Liq. Cryst.*, **15,** 479.
[9] Bouchta, A., Nguyen, H. T., Achard, M. F., Hardouin, F., Destrade, C., Twieg, R. J., Maaroufi, A., and Isaert, N., 1992, *Liq. Cryst.*, **12,** 575.
[10] Nguyen, H. T., Bouchta, A., Navailles, L., Barois, P., Isaert, N., Twieg, R. J., Maaroufi, A., and Destrade, C., 1992, *J. Phys.*, **2,** 1889.
[11] Navailles, L., Barois, P., and Nguyen, H. T., 1993, *Phys. Rev. Lett.*, **71,** 545.
[12] (*a*) Chandani, A. D. L., Ouchi, Y., Takezoe, H., Fukuda, K., Terashima, K., Furukawa, K., and Kishi, A., 1989, *Jpn. J. appl. Phys.*, **28,** 1261; (*b*) Galerne, Y., and Liebert, L., 1990, *Phys. Rev. Lett.*, **64,** 906; (*c*) Hamelin, P., Levelut, A. M., Martinot-Lagarde, P., and Liebert, L., 1993, *J. Phys. II France*, **3,** 681; (*d*) Levelut, A. M., Germain, C., Keller, P., Liebert, L., and Billard, J., 1983, *J. Phys. (Paris)*, **44,** 623.
[13] (*a*) Grandjean, F., 1922, *C.R. Acad. Sci. Paris*, **172,** 71; (*b*) Caz-no, R., 1968, *Bull. Soc. Fr. Min. Cryst.*, **91,** 20; (*c*) Bouligand, Y., 1974, *J. Phys.*, **35,** 958.
[14] Clark, N. A., and Lagerwall, S. T., 1980, *Appl. Phys. Lett.*, **36** (11), 899.
[15] Nguyen, H. T., Babeau, A., Leon, C., Marcerou, J. P., Destrade, C., Soldera, A., Guillon, D., and Skoulios, A., 1991, *Liq. Cryst.*, **9,** 253.
[16] Navailles, L., Pindak, R., Barois, P., and Nguyen, H. T., 1995, *Phys. Rev. Lett.*, **74,** 5224.
[17] Renn, S. R., and Lubensky, T. C., 1991, *Mol. Cryst. liq. Cryst.*, **209,** 349.